Available online at www.sciencedirect.com
SCIENCE DIRECT®
Journal of Solid State Chemistry 179 (2006) 130–139
JOURNAL OF SOLID STATE CHEMISTRY
www.elsevier.com/locate/jssc

Synthesis and structure of the ternary and quaternary strontium nitride halides, $Sr_2N(X, X')$ (X, X' = Cl, Br, I)

Amy Bowman[a,1], Ronald I. Smith[b], Duncan H. Gregory[a,*]

[a]*School of Chemistry, University of Nottingham, Nottingham NG7 2RD, UK*
[b]*ISIS Facility, Rutherford Appleton Laboratory, Chilton, Didcot OX11 0QX, UK*

Received 16 August 2005; received in revised form 4 October 2005; accepted 5 October 2005
Available online 15 November 2005

Abstract

A number of new, layered nitride mixed halides have been synthesised in the quaternary phase systems Sr–N–Cl–Br and Sr–N–Br–I. The variation in structure with composition has been investigated by powder X-ray and powder neutron diffraction techniques and the structure of strontium nitride iodide, Sr_2NI, has been determined for the first time (rhombohedral space group R-3m, $a = 4.0103(1)$ Å, $c = 23.1138(2)$ Å, $Z = 3$). A continuous solid solution exists between Sr_2NCl and Sr_2NBr with intermediate compounds adopting the same *anti*-α-$NaFeO_2$ structure (rhombohedral space group R-3m) as the ternary end members. A similar smooth and linear relationship between structure and composition is seen from Sr_2NBr to Sr_2NI and hence cubic close packing of metal–nitrogen layers is adopted regardless of halide, X (X'). While nitride and halide anions occupy distinct crystallographic sites, there is no ordering of the halides in the quaternary materials irrespective of stoichiometry or temperature (between 3 and 673 K).

Keywords: Synthesis; Powder X-ray diffraction; Powder neutron diffraction; Structure; Nitrides; Halides; Strontium

1. Introduction

The chemistry of inorganic nitrides has progressed rapidly over the last 15 years. It is perhaps unexpected that many of the most interesting and unusual compounds are formed by the alkali and alkaline earth elements [1,2]. The group 2 metals (A) form nitrides with A–N bonding and structures that change dramatically as one descends the group; the lighter metals (Be–Ca) form ionic, insulating or semiconducting, salt-like compounds whereas the heavier members of the group (Ca–Ba) form subnitrides with low-dimensional structures and metallic properties. The simple reaction chemistry of the subnitrides is intriguing. The layered subnitrides A_2N (A = Ca–Ba) provide a structural basis for inclusion of anions from simple spherical species such as halides to more complex, anisotropic entities such as N_2^{2-} and CN_2^{2-} [3,4]. The simplest of the families of "filled subnitrides" are the nitride halides A_2NX (X = F–I), some members of which were originally synthesised several decades ago [5–10]. Only recently, however, have the structures and properties of many of these mixed-anion compounds been revealed [11–17]. Recent work has suggested that the ternary A–N–X phase systems are more complex than originally envisaged and that the structures and anion distributions are sensitive to both the halide (X) and the conditions of synthesis [13–16]. Moreover, variation in structure and anion distribution is likely to have profound effects on electronic properties. For example, in the Mg–N–F system alone, one moves from insulating MgF_2 (calculated direct band gap, E_g, of 6.8 eV) through Mg_3NF_3 (E_g = 3.6 eV) and L–Mg_2NF (E_g = 2.1 eV) to semiconducting Mg_3N_2 with a calculated direct band gap of 1.6 eV (2.8 eV experimentally [18]). Remarkably little is known regarding the nitride halides of both the heavier alkaline earth metals and those containing the heavier halides.

In a previous communication, we presented results of our preliminary investigations of the quaternary A–N–X–X' (A = Ca, Sr; X, X' = Cl−I) systems and the

*Corresponding author. Fax: +44 115 9513563.
E-mail address: Duncan.Gregory@Nottingham.ac.uk (D.H. Gregory).
[1]Current address: Department of Chemistry, University of Liverpool, Crown Street, Liverpool L69 7ZD, UK.

0022-4596/$ - see front matter © 2005 Elsevier Inc. All rights reserved.
doi:10.1016/j.jssc.2005.10.006

discovery of the first nitride mixed halides [19]. In this paper, we extend our investigations over the entire range of composition in the $Sr_2NCl_{1-x}Br_x$ system (from $0 \leqslant x \leqslant 1$) and probe the $Sr_2NBr_{1-x}I_x$ system for the first time. The purpose of this systematic study was to follow the changes in structure and anion distribution in strontium nitride halides with stoichiometry and temperature and to perform the first structure determinations of strontium nitride iodides. Powder neutron diffraction data have provided definitive structural models for the ternary nitride halides Sr_2NCl, Sr_2NBr and Sr_2NI and for selected quaternary compounds in the respective quaternary phase systems. The variations in structure and bonding in the nitride halides are discussed and we set these within the wider context of the growing family of known A_2NX ($A = Ca$, Sr) mixed-anion compounds.

2. Experimental details

2.1. Starting materials

All manipulations were performed in an Ar- or N_2-filled glovebox. Strontium nitride Sr_2N was synthesised by the direct reaction of cleaned Sr metal (ca. 12 g cut from an ingot; Alfa, 99%) with dried nitrogen at 793 K. The metal was contained in a stainless-steel crucible and heated under N_2 (ca. 2 atm) within a closed steel vessel for 24 h. The resulting purple/black block was obtained after cooling and the identity of the ground nitride powder was confirmed by powder X-ray diffraction (PXD) by reference to the ICDD Powder Diffraction File (PDF card No. 27-855) with negligible alkaline earth oxide impurities in the products.

Binary halides, $SrCl_2$ (Alfa, 99%), $SrBr_2$ (Strem, 99%) and SrI_2 (Aldrich, 99.99 + %) were obtained commercially. The chloride and bromide were pre-dried by heating in a dynamic vacuum (10^{-4} atm) at 380 K for 14 h. The anhydrous iodide was used as received. The anhydrous nature and the purity of the halides were verified by PXD.

2.2. Nitride halide synthesis

Ternary and quaternary materials (ca. 0.5 g) were prepared by reaction of Sr_2N with the respective strontium halide(s). All manipulations were performed in a purified Ar-filled glovebox. The powders were mixed and ground in overall 2:1 ratios as described in Eq. (1) and pressed as pellets. For $X = Cl$, $X' = Br$, x was varied between 0 and 1 in 0.2 increments with $x = 0.5$ as an additional sample. For $X = Br$, $X' = I$, x was varied between 0 and 1 in 0.2 increments. Pellets were wrapped in molybdenum foil and placed within stainless-steel crucibles, which were subsequently welded closed under Ar. Crucibles were fired for 5 days at 1123 K or 1023 K for (Cl, Br) and (Br,I) samples, respectively, and cooled at 20 K h^{-1} to room temperature. Crucibles were opened in a nitrogen-filled glovebox. No reaction of the nitrides with the interior of the Mo foil (nor with the stainless-steel crucibles) was observed. Reactions yielded powders of yellow–grey Sr_2NCl, grey Sr_2NBr and grey–green Sr_2NI and intermediate compositions $Sr_2NX_{1-x}X'_x$ all of which contained a minor impurity phase of SrO:

$$2Sr_2N + (1-x)SrX_2 + xSrX'_2 \rightarrow 2Sr_2NX_{1-x}X'_x + Sr. \quad (1)$$

Larger samples (ca. 2 g) of selected composition were subsequently prepared by the same method for powder neutron diffraction experiments as detailed below.

2.3. Characterisation by powder X-ray diffraction (PXD) and scanning electron microscopy (SEM)

PXD data were collected using either a Philips XPERT $\theta-2\theta$ diffractometer with CuK_α radiation or a Bruker D8 Advance diffractometer with $CuK_{\alpha1}$ radiation. Samples were loaded in a nitrogen-filled glove box and data for air-sensitive materials were collected using custom-designed sealed sample holders [20]. Cell parameters and phase purity were evaluated from 2 h step scans over 5°–80° 2θ with step size 0.02° 2θ using DICVOL91 [21] for indexing as necessary and Philips IDENTIFY and Bruker EVA routines for phase identification. Lattice parameters were refined by least-squares fitting of PXD data. Reflections for ternary and quaternary phases could be assigned to rhombohedral space group $R\text{-}3m$ and patterns matched well to our previous data [19] and those calculated by POWDERCELL 2.3 [22] for single crystal data for Sr_2NCl [13]. Refined cell parameters for the nitride chloride were in good agreement with those reported originally for single crystals. Preliminary Rietveld refinement was performed against X-ray powder data collected over 14 h ($5° \leqslant 2\theta \leqslant 130°$; 0.02° 2θ step size). Despite collecting data in sealed sample holders, samples showed evidence of hydrolysis over the scan period (both by observation of increases in sample volume and by broadening of diffraction peaks). The derived structures were used as input for initial models in neutron refinements (see below).

Morphology of microcrystalline products was investigated by SEM using a Phillips XL 30 ESEM-FEG instrument running at 10.0–20.0 kV under nitrogen. Elemental analysis was simultaneously performed by energy dispersive analysis of X-rays (EDX), taking area and point scans of samples. The air-sensitive samples were loaded into the SEM under a stream of N_2 gas.

2.4. Structure determination from powder neutron diffraction (PND)

Time of flight (TOF) PND data were collected for ca. 2 g samples of Sr_2NCl (**1**), Sr_2NBr (**2**), Sr_2NI (**3**) and the quaternary compounds of nominal composition $Sr_2NCl_{0.5}Br_{0.5}$ (**4**) and $Sr_2NBr_{0.4}I_{0.6}$ (**5**) using the high-intensity diffractometer POLARIS at the ISIS pulsed spallation neutron source, Rutherford Appleton Laboratory, UK. Data for all compounds were collected at 298 K.

Data were also collected for samples **1**, **2** and **4** at 3 K and for sample **4** at 673 K. Diffraction data were collected using the ^{3}He tube low angle and backscattering detector banks at $<2\theta> = 35^\circ$ and $<2\theta> = 145^\circ$ and the ZnS scintillator detector bank at $<2\theta> = 90^\circ$. Samples were contained in 6 mm diameter, thin walled, cylindrical vanadium sample cans. The cans were loaded in a nitrogen-filled glove box and sealed with indium gaskets ($3 \leqslant T \leqslant 298$ K) or a copper O-ring (673 K). The structures of the nitride halides were refined following the Rietveld method using the General Structure Analysis System (GSAS) software through the EXPGUI interface [23,24]. Initial models were taken from our own indexed PXD data and refined structures. A convolution of back-to-back exponentials with a pseudo-Voigt function (peakshape function 3 within GSAS) was used to model peak shapes and the background in each case was modelled by an exponential expansion function (background function 6 within GSAS), with up to six refined coefficients, accounting for contributions at both low and high Q. Initial cycles allowed for the variation of the scale factor, background and lattice parameters. As the refinements progressed atomic positions, peak width parameters, profile coefficients, isotropic temperature factors and, for quaternary phases, halide site occupancy was introduced. Anisotropic temperature factors were refined for each site in final cycles without any loss of refinement stability. SrO was simultaneously refined as an impurity phase in the profile for each sample (yielding wt% values of: 1.9(1) for **1**, 0.7(1) for **2**, 0.9(1) for **3**, 1.2(1) for **4**, 1.0(1) for **5**). Sr_2N was included as a refined phase in refinements **1** (7.3(1) wt%), **3** (3.5(1) wt%) and **5** (4.7(2) wt%) and α-Sr was also included in **3** (3.1(2) wt%), **4** (5.3(1) wt%) and **5** (3.1(1) wt%). The presence of SrO and α-Sr can be inferred from Eq. (1). We suspect that some SrX_2 loss at elevated temperature might explain the presence of residual Sr_2N in some products. In each case, the crystal structure was refined using the neutron diffraction data collected from all three detector banks simultaneously.

2.5. Property measurements

Variable temperature magnetic susceptibility measurements were performed on samples of the ternary and quaternary materials, **1–5** (ca. 90 mg) using a Quantum Design MPMS-XL 5T SQUID magnetometer. All samples were loaded in a nitrogen-filled recirculating glovebox. Data were collected between 5 and 250 K under fields of 10^3 Oe with points at 1 K intervals between 5 and 30 and 5 K intervals from 30 to 250 K. Data were corrected for the diamagnetic contribution of the sample holders (gelatine capsules).

Two point resistivity measurements were performed on pressed pellets of **1**, **2**, and **3** using a Keithley 175A autoranging digital multimeter in a nitrogen-filled recirculating glove box at 293 K. All samples tested, however, gave resistance values above the upper limit of measurement (200 MΩ), strongly supporting the premise that the nitride halides are insulators.

3. Results and discussion

3.1. Characterisation of ternary and quaternary materials

SEM micrographs revealed that representative nitride halide samples (**1**, **3** and **4**) formed plates or irregular blocks between 20 and 50 μm across. Point scans of samples of **1** and **3** yielded Sr:X ratios approximating 2:1 consistent with the expected stoichiometry of the nitride halides. EDX data for samples of **4** gave approximate Sr:Cl:Br ratios of 4:1:1.

PXD patterns of the Sr–N–Cl–Br and Sr–N–Br–I nitride halides are shown in Figs. 1 and 2, respectively. All compounds in both the Sr–N–Cl–Br and Sr–N–Br–I

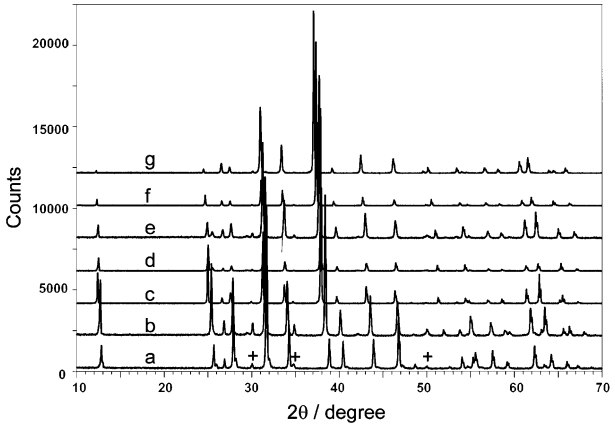

Fig. 1. PXD patterns of $Sr_2NCl_{1-x}Br_x$ nitride halides for $0 \leqslant x \leqslant 1$. Patterns shown are for (a) $x = 0$ (Sr_2NCl), (b) $x = 0.2$, (c) $x = 0.4$ (d) $x = 0.5$, (e) $x = 0.6$, (f) $x = 0.8$ and (g) $x = 1$ (Sr_2NBr). Peaks originating from an SrO impurity phase are denoted by pluses (+).

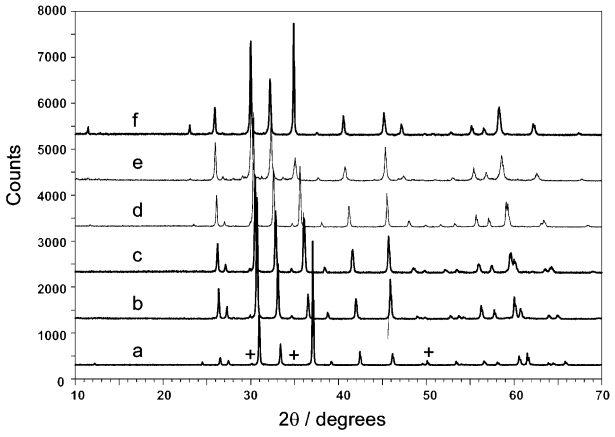

Fig. 2. PXD patterns of $Sr_2NBr_{1-x}I_x$ nitride halides for $0 \leqslant x \leqslant 1$. Patterns shown are for (a) $x = 0$ (Sr_2NBr), (b) $x = 0.2$, (c) $x = 0.4$, (d) $x = 0.6$, (e) $x = 0.8$, (f) $x = 1$ (Sr_2NI). Peaks originating from an SrO impurity phase are denoted by pluses (+).

systems could be indexed to the rhombohedral *R*-3*m* cell (isotypic to $Sr_2NCl(Br)$). Both quaternary systems show a clear trend of a peak shift to lower 2θ as the smaller halide anion is progressively replaced by its larger relative. This is commensurate with the expected increases in cell volume across the solid solutions. Both the quaternary systems show a steady, approximately linear, increase in both *a* and *c* parameters with halide content, *x* (Fig. 3). The expansion in both systems is anisotropic and enhanced along *c* compared to *a* (e.g. 10.6% expansion along *c* vs. 3.1% along a from Sr_2NCl to Sr_2NI). The corresponding *c*/*a* ratio increases from ca. 5.37 in Sr_2NCl to ca. 5.76 in Sr_2NI.

3.2. Structure

The crystallographic data and atomic parameters for the nitride halides are shown in Tables 1–4. Fitted neutron diffraction patterns following Rietveld refinement are shown in Fig. 4. Consistent with PXD experiments, Sr_2NCl, Sr_2NBr and $Sr_2NCl_{0.49}Br_{0.51}$, $Sr_2NBr_{0.41}I_{0.59}$ and Sr_2NI crystallise with the *anti*-α-$NaFeO_2$ structure. This filled *anti*-$CdCl_2$-type layered structure of the (Cl,Br) or (Br,I) compounds consists of $[NSr_2]^+$ slabs in which N is coordinated octahedrally to six Sr atoms. The layers of edge-sharing NSr_6 octahedra lie parallel to the *ab* plane stacked along the *z*-direction. The halide anions $(X, X')^-$ occupy the octahedral voids between these positively charged N–Sr layers. This thus creates alternating edge-sharing layers of NSr_6 and $(Cl,Br)Sr_6$ or $(Br,I)Sr_6$ octahedra in a cubic close packed arrangement (Fig. 5).

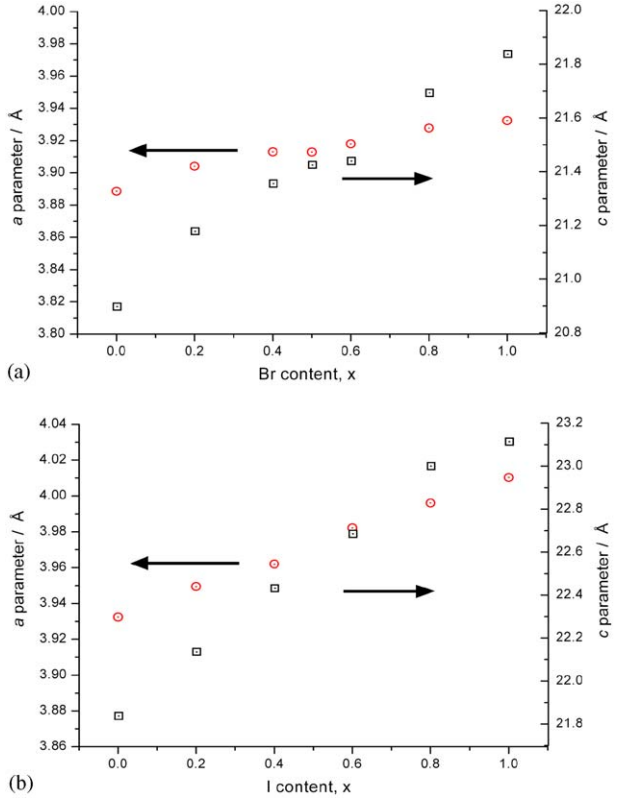

Fig. 3. Plot of variation of unit cell parameters, *a* (open circles) and *c* (open squares) against *x* for (a) $Sr_2NCl_{1-x}Br_x$ and (b) $Sr_2NBr_{1-x}I_x$ nitride halides for $0 \leqslant x \leqslant 1$.

PND data for **4** and **5** show that the halide anions in the quaternary compounds (Cl^-/Br^- and Br^-/I^-, respectively) are disordered at room temperature, statistically occupying the site between $[NSr_2]^+$ layers (octahedral 3*b* (0,0,0) site). Further, subambient and elevated temperature data for **4** demonstrate that there is no ordering of halides at 3 K and no phase transition at 673 K and hence that the α-$NaFeO_2$ structure is retained over this temperature range.

It is interesting to compare and contrast the Sr–N–*X*–*X*′ systems here with the equivalent calcium quaternary nitride halides. The strontium nitride halides exhibit a continuous field of stability for the α-$NaFeO_2$ structure from $X = Cl$ to $X = I$, yet the calcium compounds demonstrate a composition-dependent phase transition (α-$NaFeO_2$-type to β-$RbScO_2$-type) at $x \approx 0.75$ in the Ca–N–Br–I system despite comparable *c*/*a* ratios ($c/a \approx 5.65$ for $Ca_2NBr_{0.3}I_{0.7}$) [25]. One can rationalise this situation further by considering the ratio of the $[NA_2]^+$ layer thickness, *t*, to the interlayer distance, *d* (as defined by Ref. [19]; see Fig. 5). Using our PND data, the *t*/*d* ratio varies in the strontium nitride halides from 0.63 in Sr_2NCl through 0.60 in $Sr_2NCl_{0.49}Br_{0.51}$, 0.58 in Sr_2NBr and 0.54 in $Sr_2NBr_{0.41}I_{0.59}$ to 0.52 in Sr_2NI. This compares to values of 0.59 in Ca_2NCl through 0.55 in Ca_2NBr to 0.49 in Ca_2NI [25]. As in the Ca–N–*X*–*X*′ systems, *t* is essentially invariant with *X* across the range of compositions from **1** to **3** (1.8% decrease). Thus, also as in the Ca–N–*X*–*X*′ systems, the *t*/*d* ratio is effectively determined by the increasing average size of the intercalated anion rather than by changes to the relatively rigid A–N framework (*d* increases by 18.4% from **1** to **3**). Importantly, $Ca_2NBr_{0.22}I_{0.78}$ has a *t*/*d* ratio of 0.50 [25] and crystallises with the β-$RbScO_2$ structure type (i.e. HCP packing of $[A_2N]^+$ layers) and so one can envisage a critical $t/d > 0.5$ where there is a transition of HCP to CCP *A*–N layers as $[A_2N]^+$ layer repulsion becomes too great. There follows, locally, a corresponding change from XA_6 trigonal prismatic to octahedral coordination. These arguments are corroborated by an analysis of bond lengths and, significantly, bond angles as seen below.

Selected interatomic distances and angles of interest are shown in Table 5. The Sr–N bond lengths for **1**–**5** are within the range of those found in other strontium nitrides and, importantly, in close agreement to the distances found in the binary (unfilled) subnitride Sr_2N (2.6118(3) Å) [26] and, for example, the nitride diazenide, SrN [3]. The Sr–*X* bond lengths are in good agreement with data for $SrCl_2$, $SrBr_2$ and SrI_2 [27–29]. Sr–N distances in the nitride halides increase slightly with increasing halide anion radius and, for **4**, increase with temperature, as expected. The Sr–*X* distances show an approximately linear dependence with (average) halide radius across the range of quaternary compounds. From the refined bond angles (Table 5), it is apparent that the Sr–N–Sr angle, ϕ (as defined in [19]),

Table 1
Crystallographic data for $Sr_2N(X, X')$ nitride halides at 298 K

Instrument, radiation			POLARIS, neutron		
Formula	Sr_2NCl (**1**)	$Sr_2NCl_{0.49}Br_{0.51}$ (**4**)	Sr_2NBr (**2**)	$Sr_2NBr_{0.41}I_{0.59}$ (**5**)	Sr_2NI (**3**)
Crystal system			Rhombohedral		
Space group			*R*-3*m* (No. 166)		
Z			3		
M	674.1	742.4	807.5	890.0	948.5
Calculated density, ρ_X ($g\,cm^{-3}$)	4.090	4.340	4.585	4.796	4.892
Unit cell dimensions:					
a(Å)	3.8886(1)	3.9129(1)	3.9324(1)	3.9738(1)	4.0103(1)
c (Å)	20.8977(1)	21.4254(2)	21.8380(1)	22.5326(1)	23.1138(2)
V (Å^3)	273.664(2)	284.087(3)	292.455(2)	308.139(3)	321.925(3)
Observations, parameters	12433, 50	13017, 51	12408, 46	12466, 52	13338, 56
χ^2	2.62	2.78	2.91	2.73	1.53
R_{wp}	0.026	0.032	0.027	0.026	0.025
R_p	0.041	0.048	0.040	0.043	0.049

Table 2
Crystallographic data for $Sr_2N(X, X')$ nitride halides at reduced and elevated temperature

Instrument, radiation			POLARIS, neutron	
Formula	Sr_2NCl (**1**)	$Sr_2NCl_{0.49}Br_{0.51}$ (**4**)	$Sr_2NCl_{0.49}Br_{0.51}$ (**4**)	Sr_2NBr (**2**)
Crystal system			Rhombohedral	
Space group			*R*-3*m*	
Z			3	
M	674.1	742.4	742.4	807.5
Temperature (K)	3	3	673	3
Calculated density, ρ_X ($g\,cm^{-3}$)	4.122	4.380	4.247	4.627
Unit cell dimensions:				
a (Å)	3.8795(1)	3.9027(1)	3.9415(1)	3.9211(1)
c (Å)	20.8358(2)	21.3513(2)	21.6046(2)	21.7610(2)
V (Å^3)	271.574(3)	281.635(3)	290.671(4)	289.757(3)
Observations, parameters	14079, 52	13632, 51	11186, 49	12408, 46
χ^2	1.84	1.40	2.31	2.95
R_{wp}	0.013	0.013	0.024	0.015
R_p	0.024	0.031	0.039	0.031

increases with the average size of the halide and hence the $[NSr_2]^+$ layers become increasingly compressed along the *c* direction to accommodate the anion within the van der Waals gap of the subnitride structure. The changes in Sr–N–Sr and Sr–*X*–Sr angles can be compared with the equivalent angles in the calcium nitride halides by plotting against the average halide anionic radius (Fig. 6). With the switch from cubic to hexagonal close packing of $[NCa_2]^+$ layers in calcium nitride bromide iodides and the corresponding change from octahedral CaX_6 geometry to trigonal prismatic geometry, there is a commensurate step increase in ϕ (and sharp decrease in $\angle$ Ca–*X*–Ca) which is not observed over the same range of anionic radius for the Sr compounds. Also in similarity to $Ca_2N(X, X')$ compounds, there is an almost negligible variation in Sr–Sr distance across the thickness of the $[NSr_2]^+$ layers with *X* whereas the other intralayer Sr–Sr distance (in the *ab* plane) increases more significantly (ca. 3% from **1** to **3**). This trend is again a feature of the increased angular compression of the edge-sharing NSr_6 octahedra with the increasing radius of X^-.

The relation between key structural data (*c* parameter, Sr–N, Sr–*X* bond lengths) and anion type, X^-, can be set within the context of the wider family of known alkaline earth nitride halides allowing direct comparison with the Ca compounds. The trends are illustrated in Fig. 7, which also includes the unfilled subnitrides Sr_2N and Ca_2N [26,30] (where *X* = vacancy is assumed to be situated at the 3*b*, (0,0,0), site) and the nitride hydrides Ca_2NH [31] and Sr_2NH [32] for comparison. All compounds have been

Table 3
Final atomic parameters for $Sr_2N(Cl, Br)$ nitride halides

Instrument, radiation	POLARIS, neutron						
Compound	Sr_2NCl (**1**)	Sr_2NCl (**1**)	$Sr_2NCl_{0.49}Br_{0.51}$ (**4**)	$Sr_2NCl_{0.49}Br_{0.51}$ (**4**)	$Sr_2NCl_{0.49}Br_{0.51}$ (**4**)	Sr_2NBr (**2**)	Sr_2NBr (**2**)
Temperature (K)	3	298	3	298	673	3	298
Sr (6*c*) (0, 0, *z*): *z*	0.2309(1)	0.2308(1)	0.2293(1)	0.2290(1)	0.2287(1)	0.2279(1)	0.2277(1)
$100 \times U_{11} = U_{22}(Å^2)$	0.16(1)	0.68(1)	0.18(1)	0.68(1)	1.80(2)	0.22(1)	0.72(1)
$100 \times U_{33}(Å^2)$	0.20(1)	0.72(1)	0.63(2)	1.26(2)	2.52(4)	0.28(1)	0.84(1)
$100 \times U_{12}(Å^2)$	0.08(1)	0.34(1)	0.09(1)	0.34(1)	0.90(1)	0.11(1)	0.36(1)
N (3*a*) (0, 0, $\frac{1}{2}$):							
$100 \times U_{11} = U_{22}(Å^2)$	0.40(1)	0.69(1)	0.39(1)	0.67(1)	1.62(2)	0.42(1)	0.78(1)
$100 \times U_{33}(Å^2)$	0.49(2)	1.03(2)	0.90(2)	1.68(3)	3.19(5)	0.61(2)	1.08(1)
$100 \times U_{12}(Å^2)$	0.20(1)	0.34(1)	0.20(1)	0.33(1)	0.81(1)	0.21(1)	0.39(1)
(*X*,*X*′) (3*b*) (0, 0, 0):							
Occupancy (*X*)	1.0	1.0	0.48(1)	0.49(1)	0.50(1)	1.0	1.0
$100 \times U_{11} = U_{22}(Å^2)$	0.51(1)	1.55(1)	0.28(1)	1.10(1)	3.09(4)	0.29(1)	1.15(1)
$100 \times U_{33}(Å^2)$	1.05(2)	1.67(2)	0.71(3)	1.72(1)	3.33(6)	0.27(2)	1.02(2)
$100 \times U_{12}(Å^2)$	0.25(1)	0.78(1)	0.14(1)	0.55(1)	1.55(2)	0.15(1)	0.58(1)

Where $U_{iso} = 4/3[a^2U_{11} + b^2U_{22} + c^2U_{33} + ab(\cos\gamma)U_{12} + ac(\cos\beta)U_{13} + bc(\cos\alpha)U_{23}]$.

Table 4
Final atomic parameters for $Sr_2NBr_{1-y}I_y$ ($y > 0$) nitride halides

Instrument, radiation	POLARIS, neutron	
Compound	$Sr_2NBr_{0.41}I_{0.59}$ (**5**)	Sr_2NI (**3**)
Sr (6c) (0, 0, *z*): *z*	0.2746(1)	0.2764(1)
$100 \times U_{11} = U_{22}(Å^2)$	0.81(1)	0.77(1)
$100 \times U_{33}(Å^2)$	1.67(2)	0.91(2)
$100 \times U_{12}(Å^2)$	0.41(1)	0.38(1)
N (3*a*) (0, 0, $\frac{1}{2}$):		
$100 \times U_{11} = U_{22}(Å^2)$	0.80(1)	0.84(1)
$100 \times U_{33}(Å^2)$	2.05(2)	1.25(2)
$100 \times U_{12}(Å^2)$	0.40(1)	0.42(1)
(*X*,*X*′) (3*b*) (0, 0, 0):		
Occupancy (*X*)	0.41(1)	1.0
$100 \times U_{11} = U_{22}(Å^2)$	1.17(2)	0.97(1)
$100 \times U_{33}(Å^2)$	1.31(3)	1.24(3)
$100 \times U_{12}(Å^2)$	0.59(1)	0.49(1)

Where $U_{iso} = 4/3[a^2U_{11} + b^2U_{22} + c^2U_{33} + ab(\cos\gamma)U_{12} + ac(\cos\beta)U_{13} + bc(\cos\alpha)U_{23}]$.

transformed to the *R*-3*m* cell in the figure for clarity. The trends observed in the mixed halide systems (**1**–**5**) studied here and discussed above are reproduced in the extended range of $A_2N(X, X')$ compounds. The relationships in the Sr–N–*X*–*X*′ systems between anion size vs. interlayer repulsion and *c* parameters and bond lengths mirror those in the Ca compounds [25]. As in $Ca_2N(X, X')$ nitrides, the unfilled subnitride compound is located between the chloride and the hydride in terms of *c* and *A*–*X* bond length trends. As with Ca_2NF, Sr_2NF has not yet been reported with a layered (α-$NaFeO_2$) structure. However, unlike the Ca analogue, Sr_2NH forms the rhombohedral layered structure as opposed to a 3D rock salt variant (either a simple cube or a cubic superstructure). This would suggest that the α-$NaFeO_2$ structure is stabilised for larger alkaline earth atoms $A = Sr$ over $A = Ca$ for *both* larger and smaller anions, X^- ($X = I$; $t/d = 0.52$ and $X = H$; $t/d = 0.77$ for Sr_2NX).

Given the significant covalent contribution often associated with bonds between nitrogen and the less electropositive elements, application of bond valence calculations in nitride systems is best performed with caution. Nevertheless, Brese and O'Keeffe used valence sums extensively and effectively in their original classification of nitride crystal chemistry in 1992 [33]. Useful *qualitative* information can still be obtained from this approach. Bond valence sums were calculated using values from Brese and O'Keeffe [34] for a number of $Sr_2N(X, X')$ compounds and are shown in Table 6. There are several points that arise from the data. First, the valence sums of Sr and N are lower than expected for all the nitrides. These are lower than those calculated for the equivalent Ca compounds [25] and, notably, the difference between calculated and expected oxidation state is quite striking for N. The values are, however, similar to those calculated in the bond valence treatment of the doubled rock salt structured Sr_2NF where the "underbonded" nature of the Sr–N (and Sr–F)

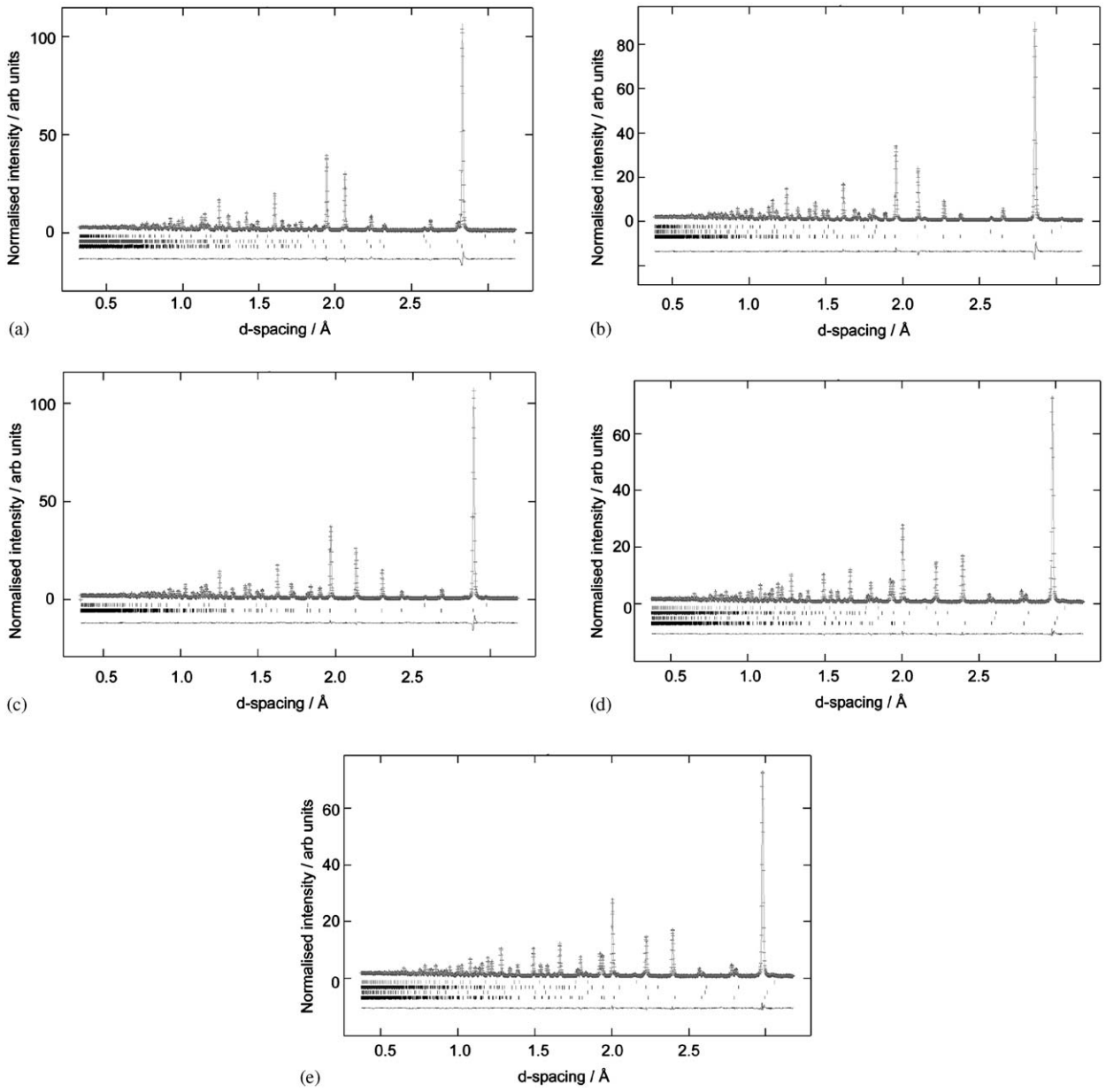

Fig. 4. Observed, calculated and difference (OCD) profile plots for the neutron refinements of (a) Sr_2NCl (**1**), (b) $Sr_2NCl_{0.49}Br_{0.51}$ (**4**), (c) Sr_2NBr (**2**), (d) $Sr_2NBr_{0.41}I_{0.59}$ (**5**) and (e) Sr_2NI (**3**) at 298 K. Crosses depict observed data whereas the solid line depicts the calculated profile. The difference profile is shown below. Tick marks below the profile mark the reflection positions for the $Sr_2N(X, X')$ phases and additional phases of SrO, α-Sr (b, d, e) and Sr_2N (a, d, e). Data collected from the backscattering detector bank ($<2\theta> = 145°$) are shown here.

environment is attributed to factors including the applicability of the method to high cation:anion ratio solids and also the role of Sr–Sr interactions [15]. Likewise, the bond valence sums for the unfilled subnitrides are lower then expected [26,30]. Second, the Sr valence is notably higher (and nearer 2) in the "filled" nitrides vs. Sr_2N. This semi-quantitatively reflects the change in bonding from $[Sr_2N]^+ \bullet e^-$ in Sr_2N to $[Sr_2N]^+(X, X')^-$ in ternary and

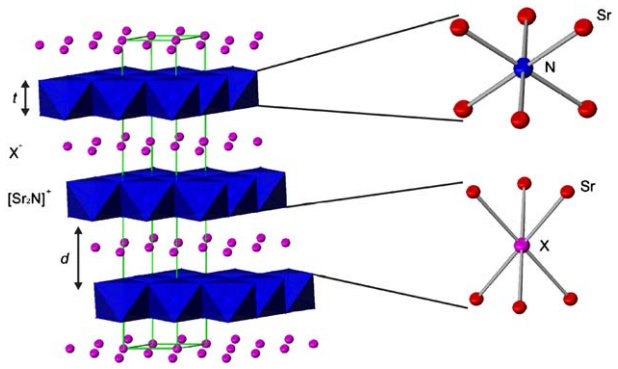

Fig. 5. Crystal structure of $Sr_2N(X, X')$ ($X, X' = Cl$, Br, I) (*anti*-α-$NaFeO_2$-type). Polyhedra are N-centred NSr_6 octahedra.

Table 5
Selected interatomic distances and angles for $Sr_2N(X, X')$ nitride halides

Compound	Sr_2NCl (1)	Sr_2NCl (1)	$Sr_2NCl_{0.49}Br_{0.51}$ (4)	$Sr_2NCl_{0.49}Br_{0.51}$ (4)	$Sr_2NCl_{0.49}Br_{0.51}$ (4)	Sr_2NBr (2)	Sr_2NBr (2)	$Sr_2NBr_{0.41}I_{0.59}$ (5)	Sr_2NI (3)
Temperature (K)	3	298	3	298	673	3	298	298	298
3 × Sr–Sr (Å)	3.4912(5)	3.4952(4)	3.4959(5)	3.5012(5)	3.5171(8)	3.4953(5)	3.5002(4)	3.5039(5)	3.5065(5)
6 × Sr–Sr (Å)	3.8795(1)	3.8886(1)	3.9027(1)	3.9129(1)	3.9415(1)	3.9211(1)	3.9324(1)	3.9738(1)	4.0103(1)
3 × Sr–N (Å)	2.6096(2)	2.6143(1)	2.6198(2)	2.6253(2)	2.6413(3)	2.6264(2)	2.6323(1)	2.6490(2)	2.6636(2)
3 × Sr–X (Å)	3.0934(2)	3.1040(2)	3.1646(2)	3.1769(2)	3.2071(4)	3.2238(3)	3.2373(2)	3.3429(2)	3.4337(2)
Sr–N–Sr (°)	96.031(8)	96.100(7)	96.294(9)	96.536(8)	96.514(1)	96.572(9)	96.656(6)	97.191(8)	97.669(8)
Sr–X–Sr (°)	77.667(7)	77.566(6)	76.139(7)	76.028(7)	75.829(10)	74.910(7)	74.798(5)	72.935(6)	71.460(6)

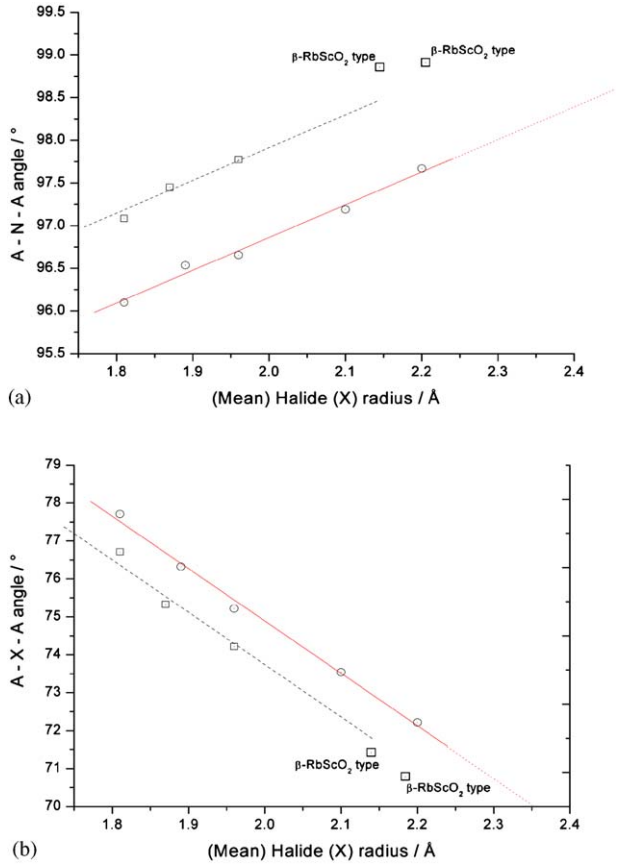

Fig. 6. Plots of (a) A–N–A angle (ϕ) and (b) A–X–A angle against mean halide anion radius for $A = Sr$ (open circles) and $A = Ca$ (open squares) ternary and quaternary nitride halides. All points represent α-$NaFeO_2$ structured nitride halides (with CCP $[A_2N]^+$ layers) unless otherwise indicated.

quaternary compounds. Third, the N valence apparently decreases from $X = Cl$ through $X = Br$ to $X = I$ (and as compared to the unfilled nitride Sr_2N) as halide electronegativity decreases from 3.0 through 2.8–2.5, respectively [35]. DFT calculations show significant covalency in the A–N layers in Sr_2NH, for example (giving an effective charge on N of ca. −1.8, which agrees well with bond valence sums) [36]. One would expect the nitride halides to become more covalent with heavier X.

3.3. Properties

Each of the ternary nitride halides display an essentially temperature independent susceptibility profile. Between 20 and 250 K weak paramagnetism is observed with corrected values of $\chi_M \sim 5 \times 10^{-4}$ emu mol^{-1} across the temperature independent region in all samples. The magnitude and temperature dependence of the molar susceptibility is very similar to that of the ''unfilled'' subnitrides [26,30]. Evidence of a slight Curie tail is observed in some samples below 20 K. This is likely attributable to low concentrations of transition metal impurities and most likely ppm quantities of steel (or respective component nitrides/oxides)

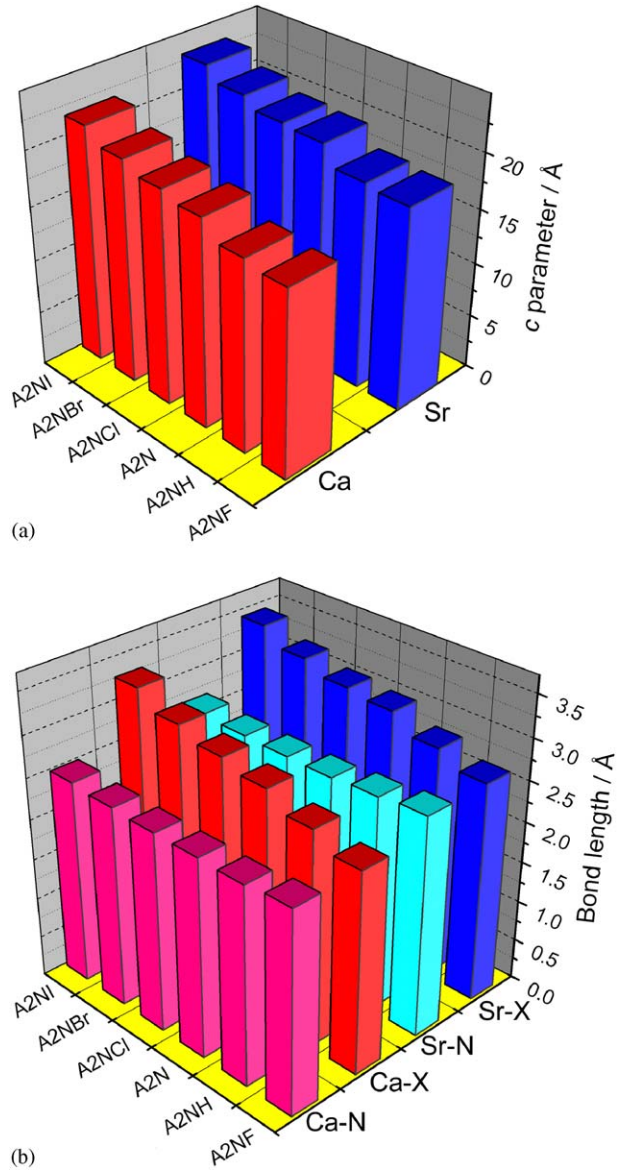

Fig. 7. Three-dimensional histogram plots depicting variation in (a) cell parameter, c and (b) A–N and A–X bond lengths for selected A_2NX nitrides (A = Sr, Ca). Note, Ca_2NH, Ca_2NF and Sr_2NF (all cubic rock salt derivatives) and Ca_2NI (*anti*-β-$RbScO_2$-type) cell parameters have been transformed to the R-3m unit cell. Sr_2N Sr_2NF and Sr_2NH values are taken from Refs. [26,10,32], respectively. Ca_2N, Ca_2NH and Ca_2NF values are taken from Refs. [30,31,10], respectively.

from the reaction crucibles. In each case these impurities are below the detection limits of PND, PXD or EDX. Given also the inevitable inclusion of low levels of strontium impurities (see Eq. (1)), then the nitride halides are almost certainly intrinsically diamagnetic which is consistent with their formulations, appearance and resistivity measurements at room temperature. Experimental investigations of the electronic properties of the nitride hydrides and halides, $A_2N(X, X')$ (A = Mg–Ba) are not extensive. Whereas both band structure calculations and experiment demonstrate that the parent subnitrides Ca_2N and Sr_2N are anisotropic metals [26,37,38], rhombohedral

Table 6
Bond valence sums for Sr_2NX nitrides

Compound	A site valence	N site valence	X site valence	Reference
Sr_2NF (*Fd*-3*m*)	1.6[a]	2.4[a]	0.8, 1.1[a]	[15]
Sr_2NF (*Fd*-3*m*)	1.6[a]	2.3[a]	0.7, 1.1[a]	[15]
$Sr_2NH(D)$	1.3	2.0	0.6	[32]
$Sr_2NH(D)$	1.5	2.5	0.6	[39]
Sr_2N	1.2[a]	2.5[a]	—	[26]
Sr_2NCl	1.7	2.1	1.2	This work
$Sr_2NCl_{0.49}Br_{0.51}$	1.7	2.1	1.3	This work
Sr_2NBr	1.7	2.0	1.3	This work
$Sr_2NBr_{0.41}I_{0.59}$	1.7	1.9	1.4	This work
Sr_2NI	1.6	1.9	1.3	This work

[a]As calculated in the original reference.

(α-$NaFeO_2$-type) Sr_2NH, for example, is a semiconductor with a calculated direct band gap of 1.6 eV [36] (although optical measurements suggest an indirect gap of 2.5 eV [32]).

4. Summary

New nitride mixed halides, Sr_2N(Cl, Br) and Sr_2N(Br, I) have been synthesised and structurally characterised by powder X-ray and powder neutron diffraction methods. The rhombohedral, α-$NaFeO_2$ structure of Sr_2NI has been determined for the first time. Both the nitride chloride bromides and nitride bromide iodides form a continuous solid solution between end members. Nitride and halides are ordered in all the ternary and quaternary nitride halides but the halide anions themselves (X, X') remain disordered in the nitride mixed halides irrespective of the halide or of the temperature investigated.

Acknowledgments

We thank the EPSRC for funding this work and the CCLRC for direct access beamtime at ISIS. We also gratefully acknowledge the University of Nottingham for a studentship for AB.

References

[1] A. Simon, Coord. Chem. Rev. 163 (1997) 253.
[2] D.H. Gregory, Coord. Chem. Rev. 215 (2001) 301.
[3] G. Auffermann, Y. Prots, R. Kniep, Angew. Chem. Int. Ed. 40 (2001) 547.
[4] O. Reckeweg, F.J. DiSalvo, Angew. Chem. Int. Ed. 39 (2000) 412.
[5] P. Ehrlich, W. Deissmann, Angew. Chem. 70 (1958) 656.
[6] P. Ehrlich, W. Deissmann, E. Koch, V. Ullrich, Z. Anorg. Allg. Chem. 328 (1964) 243.
[7] H.-H. Emons, D. Anders, R. Roewer, F. Vogt, Z. Anorg. Allg. Chem. 333 (1964) 99.
[8] H.-H. Emons, W. Grothe, H.-H. Seyfarth, Z. Anorg. Allg. Chem. 363 (1968) 191.
[9] S. Andersson, J. Solid State Chem. 1 (1970) 306.
[10] P. Ehrlich, W. Linz, H.J. Seifert, Naturwissenschaft 4 (1971) 219.

[11] C. Hadenfeldt, H. Herdejürgen, Z. Anorg. Allg. Chem. 545 (1987) 177.
[12] C. Hadenfeldt, H. Herdejürgen, Z. Anorg. Allg. Chem. 558 (1988) 35.
[13] O. Reckeweg, F.J. DiSalvo, Solid State Sci. 4 (2002) 575.
[14] R.A. Nicklow, T.R. Wagner, C.C. Raymond, J. Solid State Chem. 160 (2001) 134.
[15] T.R. Wagner, J. Solid State Chem. 169 (2002) 13.
[16] H. Sebel, T.R. Wagner, J. Solid State Chem. 177 (2004) 2772.
[17] D.R. Jack, M. Zeller, T.R. Wagner, Acta Crystallogr. C 61 (2005) i6.
[18] C.M. Fang, K.V. Ramanujachary, H.T. Hintzen, G. de With, J. Alloy Compd. 351 (2003) 72.
[19] A. Bowman, P.V. Mason, D.H. Gregory, Chem. Commun. (2001) 1650.
[20] M.G. Barker, M.J. Begley, P.P. Edwards, D.H. Gregory, S.E. Smith, J. Chem. Soc. Dalton Trans. (1996) 1.
[21] A. Boultif, D. Louer, J. Appl. Crystallogr. 24 (1991) 987.
[22] W. Kraus, G. Nolze, J. Appl. Crystallogr. 29 (1996) 301.
[23] A.C. Larson, R.B. von Dreele, The General Structure Analysis System, Los Alamos National Laboratories, Report LAUR 086-748, LANL, Los Alamos, NM, 2000.
[24] B.H. Toby, J. Appl. Crystallogr. 34 (2001) 210.
[25] A. Bowman, R.I. Smith, D.H. Gregory, J. Solid State Chem. 178 (2005) 1807.
[26] N.E. Brese, M. O' Keeffe, J. Solid State Chem. 87 (1990) 134.
[27] G. Brauer, O. Müller, Z. Anorg. Allg. Chem. 295 (1958) 218.
[28] R.L. Sass, T.E. Brackett, E.B. Brackett, J. Phys. Chem. 67 (1963) 2862.
[29] E.T. Rietschel, H. Baernighausen, Z. Anorg. Allg. Chem. 369 (1969) 62.
[30] D.H. Gregory, A. Bowman, C.F. Baker, D.P. Weston, J. Mater. Chem. 10 (2000) 1635.
[31] T. Sichla, H. Jacobs, Eur. J. Solid State Inorg. Chem. 32 (1995) 49.
[32] T. Sichla, F. Altorfer, D. Hohlwein, K. Reimann, M. Steube, J. Wrzesinski, H. Jacobs, Z. Anorg. Allg. Chem. 623 (1997) 414.
[33] N.E. Brese, M. O'Keeffe, Struct. Bonding (Berlin) 79 (1992) 307.
[34] N.E. Brese, M. O'Keeffe, Acta Crystallogr. B 47 (1991) 192.
[35] L. Pauling, The Nature of the Chemical Bond, third ed., Cornell University Press, New York, 1960.
[36] H. Smolinski, W. Weber, J. Phys. Chem. Solids 59 (1998) 915.
[37] C.M. Fang, G.A. de Wijs, R.A. de Groot, H.T. Hintzen, G. de With, Chem. Mater. 12 (2000) 1847.
[38] U. Steinbrenner, P. Adler, W. Höller, A. Simon, J. Phys. Chem. Solids 59 (1998) 1527.
[39] R. Chemnitzer, G. Auffermann, D.M. Többens, R. Kniep, Z. Anorg. Allg. Chem. 631 (2005) 1813.